Ejection Dynamics of a Simple Liquid from Individual Carbon Nanotube Nozzles

ARTICLE *in* NANO LETTERS · JUNE 2006

Impact Factor: 13.59 · DOI: 10.1021/nl060154y · Source: PubMed

2 AUTHORS, INCLUDING:

Manuel Melle-Franco
University of Minho
43 PUBLICATIONS **908** CITATIONS

SEE PROFILE

NANO LETTERS

2006
Vol. 6, No. 5
969−972

Ejection Dynamics of a Simple Liquid from Individual Carbon Nanotube Nozzles

Manuel Melle-Franco*,†,‡ and Francesco Zerbetto*,‡

Istituto Nazionale di Scienza e Tecnologia dei Materiali, Italy, and Dipartimento di Chimica "G. Ciamician", Università di Bologna, V. F. Selmi 2, 40126, Bologna, Italy

Received January 23, 2006; Revised Manuscript Received February 24, 2006

ABSTRACT

Molecular dynamics simulations show that the flow of a high pressurized atomic liquid inside carbon nanotube "pipets" occurs in one-atom-thick well-defined laminae. Fluxes and velocities at ejection are a function of the inlet diameter and the type of outlet. In the conditions investigated here, the force of the ejected liquid is similar in value to that of biomotors, while the output per second is of the order of picoliters.

In this work, we address—through molecular dynamics simulations—the issues connected to the motion of a fluid under a strong external pressure before and at ejection from twinned carbon nanotubes. In essence, we investigate the flow of liquid inside single nanotubes constructs that resemble pipets.

Two single-walled carbon nanotubes of different diameters can be seamlessly connected through intramolecular nanotube junctions; see Figure 1. These systems have been proposed as candidates for molecular-scale electronic components and, although challenging experimentally, have been observed and investigated.[1,2] Nanotubes also form endohedral complexes with a variety of molecules achieving both p- and n-type doping.[3] Liquids flow through a membrane of aligned carbon nanotubes 4−5 orders of magnitude faster than that predicted from conventional fluid-flow theory. The high fluid velocity is due to an almost frictionless interface at the carbon nanotube wall.[4]

Narrower tubes forming the *outlet* were joined to an *inlet* formed by a wider zigzag nanotube, Figure 1. Junctions connecting different helicity and/or diameter tubes are typically formed by interposing one or multiple topological defects, made by pentagons and heptagons, on the fully hexagonal carbon lattice.[5] Two different junction/nozzle shapes, symmetric and asymmetric, were considered. The asymmetric structures are more easily found experimentally[1,2] and require a junction containing one pentagon and one heptagon, parts a and c of Figure 1. Symmetric structures are unlikely to form spontaneously because they require the presence of two pentagon−heptagon pairs in precise relative positions, Figure 1b.

Since in this work both inlet and outlet are zigzag nanotubes of type (n,0), we introduce the simplified notation ($n1>n2$) or ($n1\gg n2$), where $n1$ is the first index of the wider ($n1$, 0) nanotube and $n2$ is the first index of the narrower ($n2$,0) nanotube, "$>$" represents an asymmetric junction, and "$\gg$" represents a symmetric junction. The outlet section was common to all systems (17,0). The inlet sections were (27,0), (28,0), (30,0), (33,0), (36,0), and (39,0) for the asymmetric nozzles and (27,0) and (33,0) for the symmetric ones.

Liquid argon was chosen for simplicity and computational efficiency. The methodology used for the calculations is based on the nonequilibrium molecular dynamics approach developed by Moseler and Landman for gold nanonozzles.[6] The "pipet" is held in place by freezing the initial section of the inlet, while the remaining carbons move freely. Argon is injected through the inlet in the form of a frozen cylinder cut from a simulation of the liquid quenched at the target pressure and temperature (150 K). After the initial section, but still in the inlet, in a 2 nm stretch, argon is equilibrated at 150 K. Beyond this point, the liquid is no longer equilibrated and argon atoms move according to the NVE ensemble (constant number of particles, volume and energy). An example of the system is represented in Figure 2. For efficiency, beyond certain axial/radial positions atoms are taken out from the simulation.

The potential energy functions were taken from previous work on carbon nanotubes.[7] Argon pressures ranging from 1000 to 7000 atm were tried; however, argon was found to glassify at 7000 atm, while the flux was severely reduced for pressures lower than 4000 atm. Only data for injection

* To whom correspondence may be addressed. E-mail: manuel.mellefranco@unibo.it (M.M.-F.) and francesco.zerbetto@unibo.it (F.Z.).
† Istituto Nazionale di Scienza e Tecnologia dei Materiali.
‡ Università di Bologna.

10.1021/nl060154y CCC: $33.50
Published on Web 03/31/2006

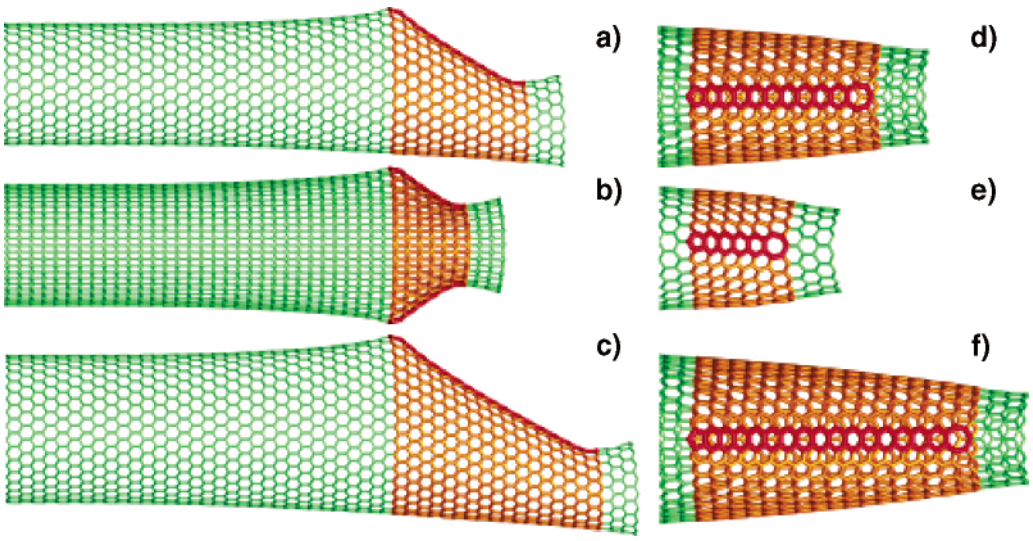

Figure 1. Carbon "pipets": (a) (27>17); (b) (27≫17); (c) (33>17); (d−f) are blow ups of the junction and outlet of the pipet on their left. Inlets and outlets are in green. Junctions are in orange with topological defects, pentagons, heptagons, and the hexagons in between, in red. Notice that in (e) there are two heptagon−pentagon stripes, but only one is visible since the second is located symmetrically on the other side of the junction.

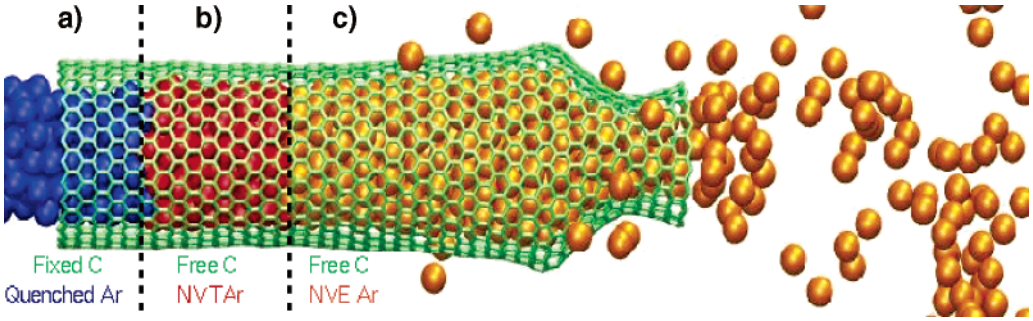

Figure 2. Snapshot of a molecular dynamics simulation showing the different parts of the model: in (a) quenched liquid argon and frozen carbon inlet section; in (b) liquid argon is equilibrated at the running temperature; in (c) the simulation is run at constant energy.

pressures of 4000, 5000, and 6000 atm are presented. Each simulation consisted of 0.7 ns of equilibration followed by, at least, 1 ns of statistical accumulation. The lack of atomic or larger scale defects in the carbon frameworks throughout the simulations, with a total run time of 0.1 ms, shows that these structures are likely to be resilient to this treatment.

The Inside Story. The argon flow was studied by calculating the average argon population at the different points of a three-dimensional grid that embeds the carbon frameworks. This analysis showed that the atoms move in laminar form or as concentric shells; see Figure 3. To the best of our knowledge, this is a unique feature of these systems and a novel finding. The laminar flow is obtained also if the carbon structure is entirely frozen and therefore appears to be a property due to the confinement. A figure that compares the fluxes of three different cases with the tube free to vibrate or frozen is given in the Supporting Information. As a rule, the tube dynamics tends to accommodate the argon flow better so that more laminas can appear.

Two qualitatively different laminar patterns were found: pure concentric layers and concentric layers with one or two central atomic lines. The number and shape of layers do not depend on the symmetry of the junction; for instance compare panels a and b and/or m and n of Figure 3. The inlet diameter mainly determines the number of concentric shells, but changes in the liquid pressure also affect the patterns, panels e and i, t, and x of Figure 3. The transitions between patterns observed by increasing diameter or pressure were the switch from (i) one-atom central flux to a two-atom flux, for instance, panels b and c of Figure 3, (ii) two-atom central flux to ring formation, for instance, compare panels o and s of Figure 3, (iii) no central one-atom flux to the presence of a central one-atom flux, for instance, compare panels t and x of Figure 3. The systems in Figure 3 were selected in order to provide examples for all of these transitions.

The mismatch between the different sizes of the carbon frameworks and the argon laminae flowing inside them can be numerically quantified by a packing index based on the dimensions of the nozzle inlet. The inverse of this value is roughly the average of interlaminar distance. Indices ranging from 2.8 layers/nm, losest packing, to 3.3 layers/nm, tightest packing, were found. The smallest values correspond to (27>17) and (39>17) at the lowest pressures, while the largest refer to the same systems at the highest pressure; see

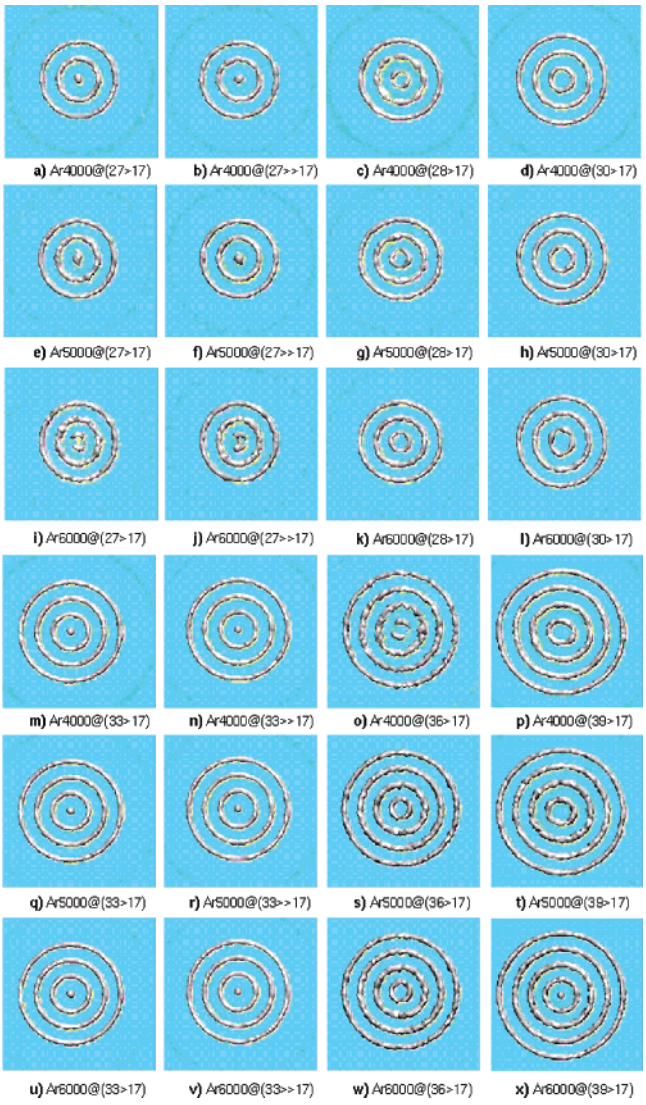

Figure 3. Inlet flow-density inside different nanonozzles, 0.125 Å^3 grid. The gray isosurfaces show the laminar flux, while the external light blue rings correspond to argon atoms that move in the opposite direction to the discharge and are parallel and external to the inlet surface (the number of these atoms is larger at lower pressures).

Table 1. Packing Indices (PI) for Different Diameter Carbon Nozzles at Different Injecting Pressures

system	inlet diameter (nm)	PI (layers/nm) 4000−5000 atm	PI (layers/nm) 6000 atm
(27>17)[a]	2.11	2.8	3.3
(28>17)	2.19	3.2	3.2
(30>17)	2.35	3.0	3.0
(33>17)	2.58	3.1	3.1
(36>17)	2.82	3.2	3.2
(39>17)[a]	3.05	2.9	3.3

[a] Nozzles where argon packing index (PI) changes with pressure. As a reference, Ar−Ar distances in bulk liquid argon decrease ~5% every 1000 atm of pressure increase.

Table 1. Interestingly, these two structures also presented consistent clogging problems in the simulations at 4000 and 5000 atm, respectively. This indicates that poor inlet/Ar commensurability, and more specifically the transition between loose and tight packing, results in clogging. Clogging was also present, although sporadically, in some of the other structures at the lowest pressure.

Table 2. Average Fluxes and Average Ar Ejection Velocities for Different Injection Pressures

system	average flux (atoms/ns) 4000 atm	5000 atm	6000 atm	Ar velocity at tip (m/s) 4000 atm	5000 atm	6000 atm
(27>17)[a]	3247	6374	7066	212	393	508
(28>17)	3429	5490	6755	226	398	478
(30>17)	3666	5461	6692	259	397	499
(33>17)[b]	2594	4483	5877	182	316	428
(36>17)	2521	4452	5728	180	329	423
(39>17)	2646	4489	5697	181	341	435
(27≫17)[a]	3571	4019	5617	269	303	419
(33≫17)[b]	1730	2861	4137	130	219	314

[a] Different junction shapes but the same inlet/outlet diameter ratios. [b] Different junction shapes but the same inlet/outlet diameter ratios.

The shape of the nozzles changes on liquid flow from elliptical when empty to a more circular when filled. Changes in the liquid pressure only slightly alter the shape of the nozzle.

The Tip of the Nozzle. The nozzle discharge is typically composed of both clusters and isolated atoms. No real jet was observed in any simulation; however, the number and size of these clusters change with nozzle geometry and inlet the pressure.

The values of the average liquid flux and/or average Ar velocity at the tip provide a relative measure of the performance of the pipets. Flux is given by the total number atoms that flow through the system divided by the length of each simulation. Average argon velocity is the average axial, i.e., parallel to the system axis, velocity of the liquid atoms at the end of the nanonozzle. The two quantities are quite but not fully equivalent. This difference supports the notion that the liquid does not flow steadily. Velocities peak at 500 m s^{-1}, while the maximum flux is of 7000 Ar atoms/ns or, macroscopically, 2×10^5 kg m^{-2} s^{-1}, for the narrowest nozzle at the largest pressure; see Table 2. A rough estimate of the thrust exerted by the liquid discharge per each structure is obtained by multiplication of the velocity and the flux to give values in the range of 10−100 pN. This is similar to the force generated and used by Nature in individual protein muscles.[8]

We have found two different regimes based on diameter, one for narrower inlets, with diameters up to 2.6 nm, where flux decreases with diameter, and one for wider inlets, with diameters from 2.6 to 3.1 nm, where flux is basically constant; see Figure 4. No correlation was found between fluxes and packing indices (only with number of laminae). The flux trend with diameter for narrower inlets can be qualitatively accounted for by considering the number of laminae in the inlet. In fact, fluxes through (27>17) and (28>17), and (30>17) and (33>17) with different numbers of layers differ. Conversely, (28>17) and (30>17) have the same number of laminae but different diameters and yield similar fluxes.

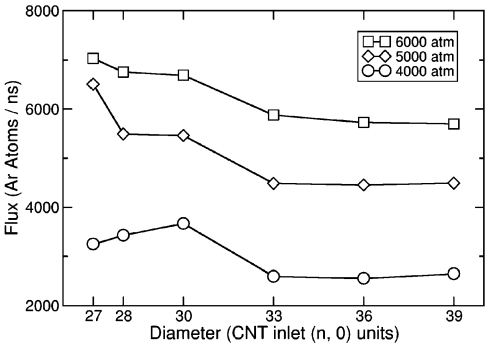

Figure 4. Flux vs inlet diameter at different pressures.

Symmetric and asymmetric nanotube "pipets" with same inlet but with different junctions differ in performance, regardless of whether they have a similar laminar flow; see for instance, panels i vs j and u vs v of Figure 3.

Symmetric structures presented, in most cases, a reduction in flux compared with the asymmetric corresponding structures with differences of up to 50%. The decrease was larger for the (33≫17) than for the (27≫17); see Table 2. Asymmetric nozzles are consequently more efficient than the steeper, symmetric nozzles. Interestingly the clogging found for the single (27>17) at 4000 atm was not observed in (27≫17).

In summary, high-pressurized liquid argon flows inside carbon "pipets" in one-atom-thick well-defined laminae. Inconmensurability between these laminae and the nozzle inlet induces clogging. Fluxes and velocities at ejection are a function of the inlet diameter and the type of outlet. Two applications of nanotubes pipets come to mind: the first is to exploit the force, similar in value to that of biomotors, of the ejected liquid for propulsion, the second is to exploit the dispensing of the "pipets" which is of the order of picoliters per second, which in turn would make possible depositions of subfemtoliter quantities that is well below the present technological limit of inkjets.

Acknowledgment. Partial support from FIRB project "Carbonio Micro e Nanostrutturato" is gratefully acknowledged.

Supporting Information Available: A description of additional computational details and a figure that compares the fluxes of three different cases with the tube free to vibrate or frozen. This material is available free of charge via the Internet at http://pubs.acs.org.

References

(1) Ouyang, M.; Huang, J. L.; Cheung, C. L.; Lieber, C. M. *Science* **2001**, *291*, 97. Hashimoto, A.; Suenaga, K.; Gloter, A.; Urita, K.; Iijima, S. *Nature* **2004**, *430*, 2004.

(2) (a) Mani, R. C.; Li, X.; Sunkara, M. K.; Rajan, K. *Nano Lett.* **2003**, *3*, 671−673. (b) Bhimarasetti, G.; Sunkara, M. K.; Graham, U. M.; Davis, B. H.; Suh, C.; Rajan, K. *Adv. Mater.* **2003**, *15*, 1629. (c) Svensson, K.; Olin, H.; Olsson, E. *Phys. Rev. Lett.* **2004**, *93*, 145901. (d) Chico, L.; Crespi, V. H.; Benedict, L. X.; Louie, S. G.; Cohen, M. L. *Phys. Rev. Lett.* **1996**, *76*, 971.

(3) Takenobu, T.; Takano, T.; Shiraishi, M.; Murakami, Y.; Ata, M.; Kataura, H.; Achiba, Y.; Iwasa Y. *Nat. Mater.* **2003**, *2*, 683−688.

(4) Majumder, M.; Chopra, N.; Andrews, R.; Hinds, B. J. *Nature* **2005**, *438*, 44; erratum, page 930.

(5) Saito, R.; Dresselhaus, G.; Dresselhaus, M. S. *Physical Properties of Carbon Nanotubes*; Imperial College Press: London, 1998.

(6) Moseler, M.; Landman, U. *Science* **2000**, *289*, 1165.

(7) Pfeiffer, R.; Kuzmany, H.; Pichler, T.; Kataura, H.; Achiba, Y.; Melle-Franco, M.; Zerbetto, F. *Phys. Rev. B* **2004**, *69*, 035404/1−035404/7. Melle-Franco, M.; Kuzmany, H.; Zerbetto, F. *J. Phys. Chem. B* **2003**, *107*, 6986−6990. Melle-Franco, M.; Prato, M.; Zerbetto, F. *J. Phys. Chem. A* **2002**, *106*, 4795−4797.

(8) Finer, J. T.; Simmons R. M.; Spudich, J. A. *Nature* **1994**, *368*, 113−119.

NL060154Y